



# Photoelectrochemical reduction of dissolved carbon dioxide over Ni(OH)<sub>2</sub> into organic oxygenates

Ahmad Nazeer Che Mat<sup>1</sup> · Wan Jeffrey Basirun<sup>1,2</sup> · Muhammad Mehmood Shahid<sup>3</sup>

Received: 14 June 2020 / Accepted: 26 November 2020 / Published online: 2 January 2021  
© Iranian Chemical Society 2021

## Abstract

The hydrothermal method has been used to prepare Ni(OH)<sub>2</sub> photocathode. The photoelectrochemical (PEC) reduction of CO<sub>2</sub> over Ni(OH)<sub>2</sub> has been conducted in 0.2 M LiClO<sub>4</sub> in aqueous and N,N-dimethylformamide (DMF) medium under visible light irradiation. The thin film was characterized by XRD, UV–Vis, FTIR, FESEM-EDX, BET analysis, and electrochemical method for the determination of phases, bandgap energy, chemical bonding, surface morphology, elemental compositions, surface area, and electrochemical properties, respectively. Based on UV–Vis spectroscopy, the bandgap energy of Ni(OH)<sub>2</sub> was 1.8 eV which enabled efficient visible light absorption for the photoreaction. The photocurrent density in aqueous and DMF solution at 0.2 V (vs. Ag/AgCl) was 24 mA cm<sup>-2</sup> and 5 mA cm<sup>-2</sup>, respectively. Acetaldehyde and methanol are the products in aqueous solution, while formic acid and methanol are the products in DMF, after 6 h of photoelectrolysis. The product formations from the photoelectrochemical reduction of dissolved CO<sub>2</sub> were 612 and 854 ppm in aqueous and DMF, respectively, where the Faradaic efficiency in aqueous and DMF is 24 and 33%, respectively. Furthermore, throughout the PEC study, the transformation of Ni(OH)<sub>2</sub> to NiO plays a significant role in the formation of organic oxygenates from the reduction reaction of CO<sub>2</sub>.

---

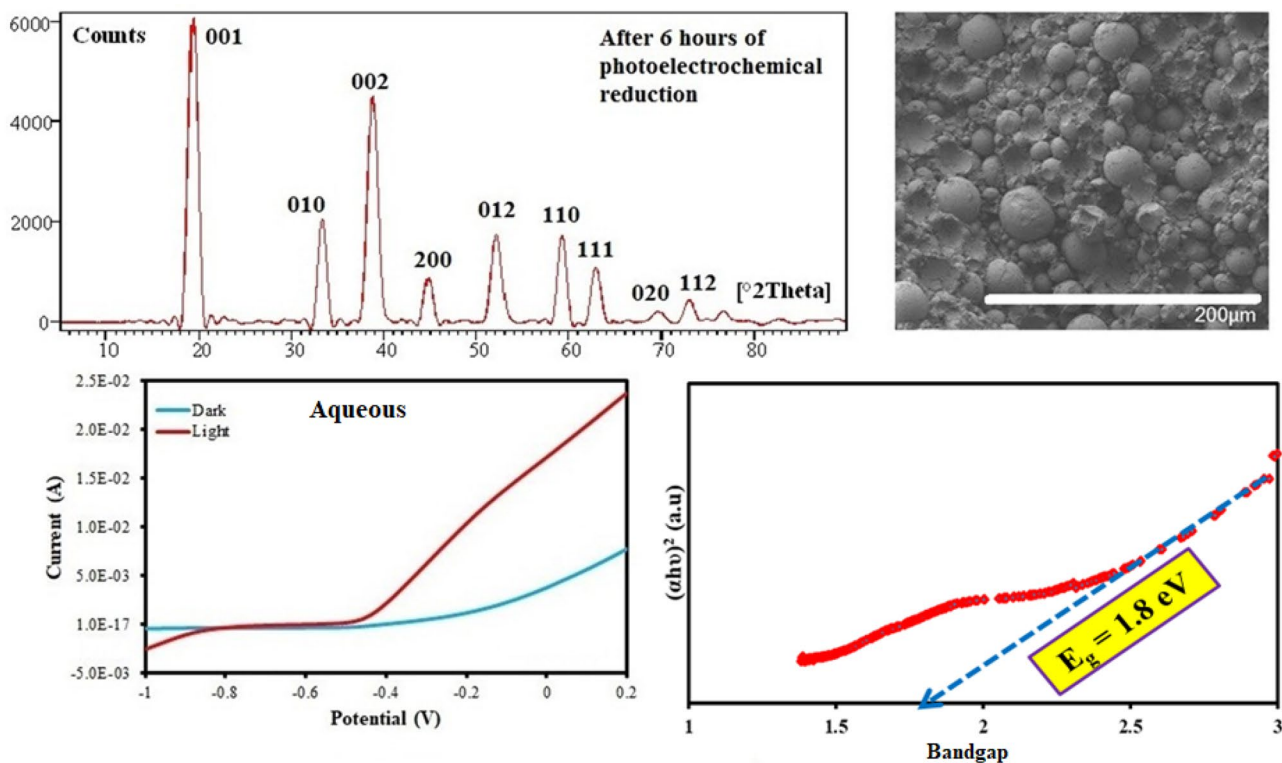
**Supplementary Information** The online version of this article (<https://doi.org/10.1007/s13738-020-02117-4>) contains supplementary material, which is available to authorized users.

---

✉ Ahmad Nazeer Che Mat  
hmd\_naz@yahoo.com

- <sup>1</sup> Department of Chemistry, Faculty of Science, University of Malaya, 50603 Kuala Lumpur, Malaysia
- <sup>2</sup> Nanotechnology and Catalysis Centre (NanoCat), Institute of Post-Graduate Studies Building, University of Malaya, 50603 Kuala Lumpur, Malaysia
- <sup>3</sup> Micro-Nano System Center, School of Information Science and Technology (SIST), Fudan University, Shanghai 200433, China

## Graphic abstract



**Keywords** Ni(OH)<sub>2</sub> · Photoelectrocatalysis · CO<sub>2</sub> reduction · C<sub>2</sub> products · Electrolyte medium

## Introduction

The major issues which need to be addressed nowadays are regarding energy and environmental crisis where the photo-conversion of CO<sub>2</sub> into carbohydrates in the manifestation of sunlight by plants could be one of the exit plans which inspired researchers to exploit atmospheric CO<sub>2</sub> as a feed-stock for the production of synthetic fuels. The focus toward artificial photosynthesis such as photocatalytic water splitting into H<sub>2</sub> and O<sub>2</sub>, in addition to the photoelectrocatalytic conversion of CO<sub>2</sub> into fuels such as methanol and formic acid or even higher carbon content products have gained momentum in the past decades. One of the recompenses of photocatalytic and photoelectrocatalytic conversion of CO<sub>2</sub> into valuable organic products is that these processes convert atmospheric CO<sub>2</sub> directly into the fuel rather than converted into carbohydrates, which is then converted into short-chain alcohols as biofuels by fermentation.

Numerous semiconductor photocatalysts have been utilized for the photo-conversion process such as TiO<sub>2</sub> [1], Co<sub>3</sub>O<sub>4</sub> [2], and Cu<sub>2</sub>O [3], but the efficiency of CO<sub>2</sub> conversion is still far beyond expectation for industrial and practical applications due to the existence of hydrogen evolution

reaction (HER) as a competitive and favorable reaction as compared to CO<sub>2</sub> reduction reaction. Additionally, most of the metal oxide photocatalysts as aforementioned suffer from wide bandgap energy making them to be more active in ultraviolet rather than visible light. Hence, new strategies such as doping with metal [4], nonmetal [5], and organic–inorganic dye sensitizations [6] have been implemented in order to enhance the efficiency of the photocatalytic reaction. Additionally, developing photocatalysts with the Z-scheme mechanism to enhance photogenerated charge carriers separation has to turn out to be research inclinations in recent times in order to optimize the photocatalytic activity. This is because the less energetic electrons from the conduction band from one of the semiconductors will recombine with photogenerated holes from the valance band of another semiconductor leaving strongly reductive electron and strongly oxidative holes in different semiconductors. The strongly reductive electrons may react with CO<sub>2</sub> for further reduction reaction, while strongly oxidative holes will undergo oxidation reaction of water into H<sub>2</sub> and O<sub>2</sub>. Hence, the z-scheme mechanism is seen to be a better strategy to minimize competitive reaction between water oxidation and CO<sub>2</sub> reduction where the photogenerated charge carriers can

be utilized as maximum as possible for both reduction and oxidation reactions.

Metals with low hydrogen evolution reaction (HER) overpotentials such as Ni, Ti, Pt, and Fe are efficient electrocatalysts for the HER process but have strong CO adsorption which is important for the reduction of CO<sub>2</sub> [7–11]. Lately, Ni-based catalyst such as Ni(OH)<sub>2</sub> as a p-type semiconductor has been utilized in various applications because of its naturally abundance, cheap, and less toxic [12]. Ni(OH)<sub>2</sub> has received increasing attention as batteries [13], direct oxidation of carbohydrates [14], supercapacitor [15], water splitting [16], and sensor [17]. However, Ni(OH)<sub>2</sub> is among the most prevalent photocatalyst for water oxidation or H<sub>2</sub> evolution reaction due to the remarkable ability of Ni(OH)<sub>2</sub> to chemisorb H<sub>2</sub>O molecule thus facilitating the cleavage of HO-H bond which is conducive to Volmer step of H<sub>2</sub> evolution reaction [18]. The use of Ni(OH)<sub>2</sub> as H<sub>2</sub> evolution photocatalyst can be obtained from several studies in the literature; for example, Ioannis et al. [19] demonstrated that the high surface area mesoporous network containing 10 wt% of Ni(OH)<sub>2</sub> modified with CdS was suitable for the generation of H<sub>2</sub> in 5 M NaOH + 10 v/v % ethanol as a sacrificial agent with an apparent quantum yield of 72%. A better H<sub>2</sub> evolution rate of 1.4 mmol/h over the as-prepared catalyst was reported due to the strong electronic coupling and charge transfer states at CdS/Ni(OH)<sub>2</sub> heterojunctions. Furthermore, instead of water splitting, the photodecomposition of organic dyes has been reported by Abdallah et al. [20] by using Ni(OH)<sub>2</sub>/BiVO<sub>4</sub>. The author reported that incorporation of 0.5 wt% Ni(OH)<sub>2</sub> exhibits the optimum quantum yield of 96% with a reaction rate constant of 1.9572 h<sup>-1</sup> within 90 min. The fabrication of ternary photocatalyst, namely Ni(OH)<sub>2</sub>/GO/TiO<sub>2</sub>, has been prepared by Barakat et al. [21] for the degradation of 2-chlorophenol which successfully removed 80% of the pollutant from the wastewater of 25 mg/L concentration within 4 h at pH 6.0.

However, only a few research works on the photoreduction of CO<sub>2</sub> have been done by implementing Ni(OH)<sub>2</sub> that can be found from literature. For example, a hybrid nanocomposite of Ni(OH)<sub>2</sub>/TiO<sub>2</sub> in an aqueous medium leads to the formation of CH<sub>4</sub> with a photoreduction rate of 2.20 μmol/g<sub>cat</sub>.h with 0.5 wt% Ni(OH)<sub>2</sub> loading, while the photoreduction rate decreased to 0.58 and 0.37 μmol/g<sub>cat</sub>.h for methanol and ethanol, respectively, with 15 wt% Ni(OH)<sub>2</sub> loading. The presence of Ni(OH)<sub>2</sub> in the nanocomposites increases the selectivity of the product besides acting as the co-catalyst [22]. Another recent study of photoreduction of CO<sub>2</sub> over Ni(OH)<sub>2</sub>/graphene was conducted by Siva et al. [23] over different types of electrolytes, namely NaHCO<sub>3</sub>, KHCO<sub>3</sub>, and NaCO<sub>3</sub> in an aqueous medium to produce CO. Their report stated that NaHCO<sub>3</sub> is a better choice of electrolyte for the formation of CO as compared to other electrolytes. However, details report on the role of

Ni(OH)<sub>2</sub> for the formation of CO from the photoreduction of CO<sub>2</sub> has not been discussed so far. Another investigation of photoreduction of CO<sub>2</sub> into CO also has been reported by Lei et al. [24] over Cu/Ni(OH)<sub>2</sub> in 0.5 M KHCO<sub>3</sub> against the reversed hydrogen electrode (RHE). Even though the formation of CO reached the Faradaic efficiency of 92% with photocurrent density of 4.3 mA/cm<sup>2</sup>, least courtesy has been rewarded to the function of Ni(OH)<sub>2</sub> and reaction mechanism of photocatalytic reduction of CO<sub>2</sub> instead of the importance of Cu has been acknowledged a lot. The most recent report by Akple et al. [25] regarding the photocatalytic reduction of CO<sub>2</sub> that has been performed over honeycomb-like graphitic carbon nitride (g-C<sub>3</sub>N<sub>4</sub>) modified Ni(OH)<sub>2</sub> suggests the formation of methane and methanol with photocatalytic activity of 1.48 and 0.73 μmol h<sup>-1</sup> g<sup>-1</sup>, respectively, which is 3.5 and 4.3 times higher than bare g-C<sub>3</sub>N<sub>4</sub> and Ni(OH)<sub>2</sub>, correspondingly. However, the photocatalytic reaction condition, the reaction mechanism, the importance of Ni(OH)<sub>2</sub>, and the quantum yield for the formation of the photocatalytic reduction of CO<sub>2</sub> were not clearly emphasized.

Thus, motivated by the above literature on photocatalytic reduction of CO<sub>2</sub> over Ni(OH)<sub>2</sub>, this manuscript intends to investigate further the importance of using Ni(OH)<sub>2</sub> in producing valuable organic oxygenates products for the energy generation from CO<sub>2</sub> gas. The mechanism in the formation of higher hydrocarbon than mainly CO as reported before such as formic acid, methanol, ethanol, and acetaldehyde in aqueous and DMF will be discussed with better photocurrent density is also reported due to alkalinity of Ni(OH)<sub>2</sub> which plays significant role in capturing acidic CO<sub>2</sub>, thus reducing the gas into valuable chemicals. Besides, the transformation of Ni(OH)<sub>2</sub> into NiO after photoelectroreduction of CO<sub>2</sub> shows an important part in constructing valuable organic product also will be acknowledged as an innovative and novel strategy in this current manuscript. Therefore, from the author's point of view and knowledge, based on the previous publications on Ni(OH)<sub>2</sub> for the photoreduction of CO<sub>2</sub>, the significant of the present manuscript highlights more on the importance of the transformation of Ni(OH)<sub>2</sub> to NiO in assisting the reduction reaction, the effect of reaction medium on the final product(s), and reaction mechanisms which are not clearly discussed by the previous report as aforementioned above.

The 'CO<sub>2</sub><sup>-</sup> radical anion is the product between the reaction of the excited electron in the conduction band and the dissolved CO<sub>2</sub>. This 'CO<sub>2</sub><sup>-</sup> radical anion is the precursor for the initial formation of formic acid. We propose a mechanism involving the hydroxyl radical 'OH in contrast to the mechanism proposed by Habisreutinger et al. [26] which involves the hydrogen radical 'H and 'CO<sub>2</sub><sup>-</sup> radical anion which is responsible for the formation of formic acid. The second driving force for the reduction of dissolved CO<sub>2</sub> is the presence of OH in the Ni(OH)<sub>2</sub>. It was proven from the

XRD, the conversion of  $\text{Ni}(\text{OH})_2$  into  $\text{NiO}$  after 6 h of electrolysis in the presence of light illumination. Again we proposed a mechanism for the reduction of dissolved  $\text{CO}_2$  with the loss of  $\text{H}_2\text{O}$  from the  $\text{Ni}(\text{OH})_2$  involving the hydroxyl radical  $\cdot\text{OH}$  for the initial formation of the formic acid precursor. While the 6 h of photoelectrolysis of dissolved carbon dioxide in an aqueous solution produces methanol (from the further reduction of formic acid) as an expected outcome, the formation of acetaldehyde as the major component is somewhat rare. In contrast, the photoelectrolysis of dissolved carbon dioxide in DMF only produces formic acid as the major product, while methanol is the minor product which is due to the lower concentration of reducing agents, which is confirmed by the low pH after 6 h of reaction. Unlike the results of this paper, most photocatalytic and photoelectrocatalytic reactions involving the reduction of dissolved  $\text{CO}_2$  in aqueous solution only report the conversion into single-carbon products such as methanol and formic acid.

## Experimental methods

Lithium perchlorate ( $\text{LiClO}_4$ ) was purchased from Sigma-Aldrich, *N,N*-dimethylformamide (DMF) was procured from Merck, and nickel nitrate hexahydrate ( $\text{Ni}(\text{NO}_3)_2 \cdot 6\text{H}_2\text{O}$ ) was attained from Fisher Scientific. Nickel (II) hydroxide was prepared by dissolving 0.60 g  $\text{Ni}(\text{NO}_3)_2 \cdot 6\text{H}_2\text{O}$  and 0.25 g urea in 100 ml distilled water under continuous stirring for two hours. The mixture was autoclaved at 100 °C for 12 h. The green powder was washed with distilled water several times and dried in an oven at 90 °C. The  $\text{Ni}(\text{OH})_2$  electrode films were fabricated by pressing the  $\text{Ni}(\text{OH})_2$  powders with acetylene black and poly(vinylidene) fluoride (PVDF) binder with the ratio of 8:1:1.

XRD was attained between  $2\theta$  of 5° and 90° using PANalytical EMPYREAN over  $\text{Cu K}_{\alpha 1}$  radiation with a step size of 0.01°. PL was acquired by the Micro-Raman PL system (Renishaw, UK) with a wavelength of 325 nm from a He-Cd laser source. FTIR was recorded on a Perkin Elmer 400FTIR/FT-FIR spectrometer from 4000–200  $\text{cm}^{-1}$ . The surface analysis was obtained using FESEM-EDX SU8220 Hitachi. The products were analyzed using Shimadzu GCMS with DB-WAX column (30 m length  $\times$  0.25  $\mu\text{m}$  thickness  $\times$  0.25 mm diameter).

The PEC performance was studied by PGSTAT30 Autolab potentiostat/galvanostat (Ecochemie, Netherlands) in an aqueous and DMF solution of 0.2 M  $\text{LiClO}_4$  after  $\text{CO}_2$  bubbling for an hour where the counter and reference electrodes were Pt wire and  $\text{Ag}/\text{AgCl}$ , respectively. The potential range of LSV was from  $-1.0$  to  $+0.2$  V vs.  $\text{Ag}/\text{AgCl}$  at 50  $\text{mV s}^{-1}$  and chronoamperometry at  $-0.5$  V vs  $\text{Ag}/\text{AgCl}$  with 150 W

Xe lamp as the light source. The method of calculating the amount of dissolved  $\text{CO}_2$  is given in the ESI.

## Results and discussions

### Material characterization

X-ray powder diffraction (Fig. 1) shows the  $2\theta$  of  $\text{Ni}(\text{OH})_2$  at 19.1°, 33.1°, 38.5°, 51.6°, 59.1°, 62.6°, 69.1°, and 72.4° which correspond to (001), (010), (002), (012), (110), (111), (020), and (112) planes, respectively. The crystallite size measured by the Debye–Scherrer's formula  $D = K\lambda/\beta \cos \theta$  gives the value of 11.2 nm, where  $D$  is the crystallite size;  $K$  is constant (0.94);  $\lambda$  is 1.54056 Å;  $\beta$  is FWHM; and  $\theta$  is the diffraction angle. The diffraction pattern matches closely with the theophrastite mineral, with a crystal system and space group of hexagonal and P-3 m1, correspondingly. The other parameters of  $\beta\text{-Ni}(\text{OH})_2$  that can be attained from powder X-ray diffraction pattern are  $a = b = 3.1300$  Å and  $c = 4.6300$  Å, while  $\alpha = \beta = 90^\circ$  and  $\gamma = 120^\circ$  [ICDS code no. 98-002-8101]. After 6 h of photoelectrochemical reduction of  $\text{CO}_2$ , some  $\text{Ni}(\text{OH})_2$  are converted into  $\text{NiO}$  (Fig. 1), with the presence of  $2\theta$  peak at 45° attributed to the (200) of  $\text{NiO}$ .

The optical characteristics of the  $\text{Ni}(\text{OH})_2$  film (Fig. 2a) shows a broad visible absorption range from 550 to 750 nm with the calculated bandgap energy of 1.8 eV from the

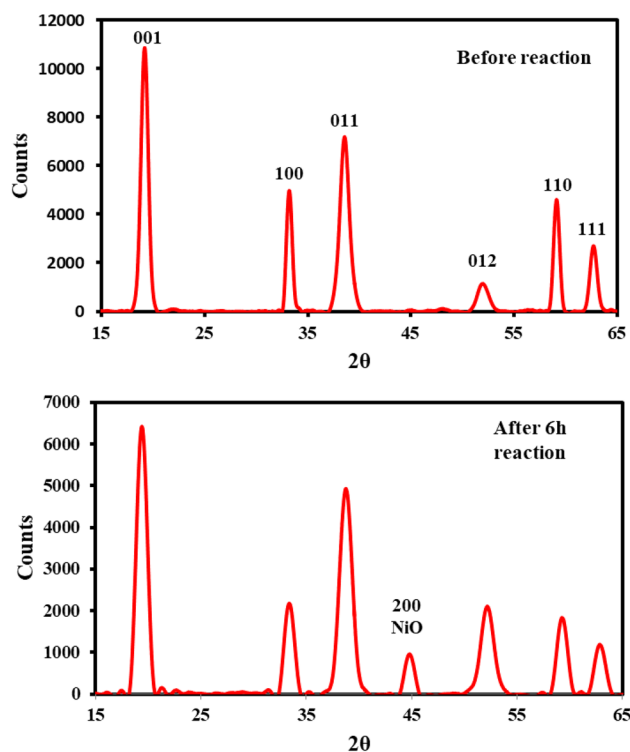
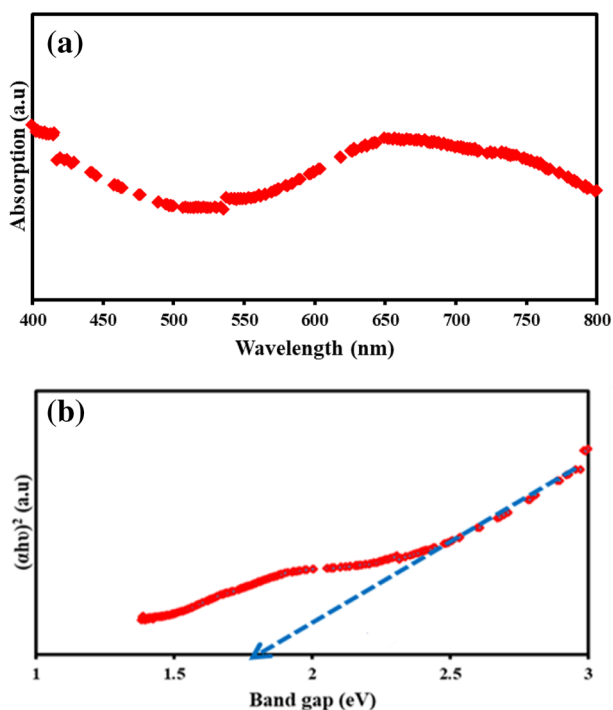


Fig. 1 XRD spectrum of  $\text{Ni}(\text{OH})_2$  film before and after 6 h reaction



**Fig. 2** a UV-Vis spectrum and b Tauc's plot of Ni(OH)<sub>2</sub>

Tauc's plot (Fig. 2b). Additionally, based on the calculated bandgap of Ni(OH)<sub>2</sub> as aforementioned above, the conduction band edge ( $E_{CB}$ ) and valance band edge ( $E_{VB}$ ) of Ni(OH)<sub>2</sub> can be determined by using the formula given below as indicated in Eqs. 1 and 2 [27]:

$$E_{CB} = \chi - E^c - 0.5E_g \quad (1)$$

$$E_{VB} = E_{CB} + E_g \quad (2)$$

where  $\chi$  is electronegativity of semiconductor,  $E^c$  is constant (4.5 eV) [28], and  $E_g$  denotes the bandgap of semiconductors

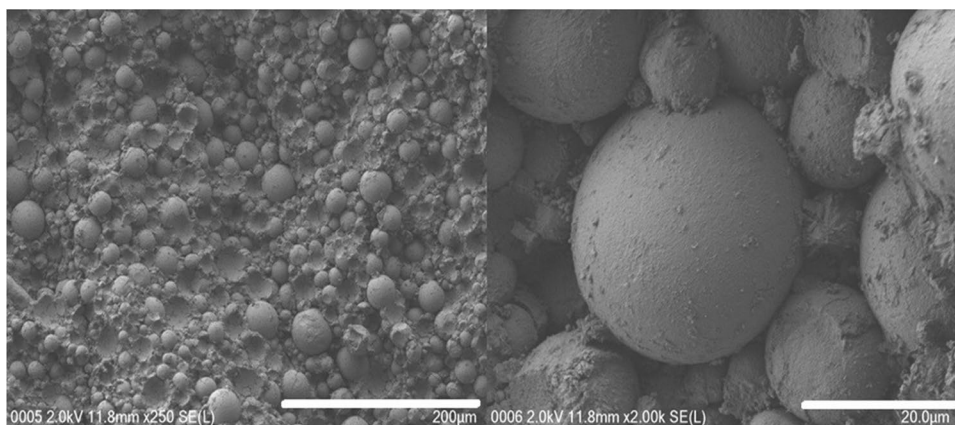
which give the value of 2.99, -2.41, and -0.6 eV for  $\chi$ ,  $E_{CB}$ , and  $E_{VB}$  of Ni(OH)<sub>2</sub>, respectively.

The PL spectrum (Fig. S1, electronic supporting information, ESI) of Ni(OH)<sub>2</sub> microparticles shows three peaks centered at 412, 547, and 677 nm. These peaks can be assigned as the electronic transition of Ni<sup>2+</sup> ion, namely  ${}^1T_{2g}(D) \rightarrow {}^3A_{2g}(F)$  and  ${}^1T_{2g}(D) \rightarrow {}^3T_{2g}(F)$ . These values are close to the bandgap value of 1.73 eV by Qi et al. from ultraviolet-visible measurements [29], which was due to the electronic transition from the  ${}^3A_{2g}$  to  ${}^3T_{2g}$  level. They also reported a larger bandgap value of 2.95 and 3.22 eV for nanoplates of Ni(OH)<sub>2</sub> with a thickness between 20 and 50 nm. The larger bandgap is due to the quantum confinement effect when the particle sizes become smaller [29–31].

The FTIR of Ni(OH)<sub>2</sub> is indicated in Fig. S2, ESI. The sharp peak at 3622 cm<sup>-1</sup> is allocated to the stretching vibration of the O–H stretching mode, which is characteristic of the free O–H group of the brucite-like structure [32]. Meanwhile, a peak at 1631 cm<sup>-1</sup> indicates the bending vibration mode of water molecules [33]. The asymmetric and symmetric stretching of NO<sub>3</sub><sup>-</sup> ion can be observed at around 1384 cm<sup>-1</sup> and 1000 cm<sup>-1</sup>, correspondingly [34–36]. While the peaks at 503 and 524 cm<sup>-1</sup> are attributed to the bending vibration of the water molecule and Ni–O(H) stretching vibration which are the characteristics of Ni(OH)<sub>2</sub>, respectively [37–40]. Additionally, a weak peak at 450 cm<sup>-1</sup> is attributed to the lattice vibration of the Ni–O bond which is in accordance with the published literature [41].

The FESEM image (Fig. 3) of Ni(OH)<sub>2</sub> reveals a spherical and smooth morphology. The morphological image of Ni(OH)<sub>2</sub> shows agglomeration of many crystallites with good dispersion of the spherical Ni(OH)<sub>2</sub> particles. The better dispersion of the particles provides adequate surface area for the adsorption of CO<sub>2</sub> for further photoelectrochemical reduction reaction to take place which might enhance the efficiency of the CO<sub>2</sub> reduction reaction. Furthermore, the spherical and compact structure of Ni(OH)<sub>2</sub> probably could be able to help in reflecting the incident light

**Fig. 3** FESEM images of Ni(OH)<sub>2</sub>

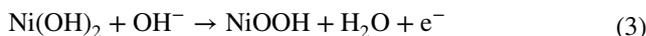


thus maximizing the utilization of visible light for further improvement of photocatalytic reduction of CO<sub>2</sub>. The elemental composition of Ni(OH)<sub>2</sub> is shown from EDX analysis (Fig. S3, ESI). The N<sub>2</sub> adsorption–desorption behavior is shown in (Fig. S4a, ESI). The sample presents a type IV isotherm with an apparent hysteresis loop between 0.5–1.0 P/P<sup>o</sup>, according to the Brunauer–Deming–Deming–Teller (BDDT) classification, indicating the presence of mesopores (2–50 nm). The hysteresis loop of Ni(OH)<sub>2</sub> represents a type of H1 behavior, which suggests the presence of a narrow distribution of uniform cylindrical pores [42]. (Figure S4b, ESI) shows the BET plot of spherical Ni(OH)<sub>2</sub> nanoparticles. The total surface area of the Ni(OH)<sub>2</sub> spherical particles is 18.9 m<sup>2</sup> g<sup>-1</sup>, from the multipoint BET equation. The pore width distribution from the desorption branch of N<sub>2</sub> isotherms by the Barrett–Joyner–Halenda (BJH) method shows a pore width and pore volume of 14.7 nm and 0.02 cm<sup>3</sup> g<sup>-1</sup>, respectively, confirming the presence of mesopores (Fig. S4c, ESI).

### Photoelectrochemical reduction of dissolved CO<sub>2</sub>

In an aqueous solution, the photoelectrochemical oxidation against Ag/AgCl as a reference electrode begins at -0.48 V with a maximum photocurrent density of 24 mA cm<sup>-2</sup> (0.2 V) under visible light irradiation as compared to the dark condition, while in DMF solution, the photoelectrochemical oxidation starts at -0.61 V. The photocurrent density under visible light irradiation in DMF is maximum at 5 mA cm<sup>-2</sup> (0.2 V) which is higher than in the dark condition, but still lower than in the aqueous solution. The control experiments were conducted on acetylene black (Fig.

S5, ESI) without the presence of CO<sub>2</sub> gas in aqueous and DMF solution. The results showed that without the presence of CO<sub>2</sub>, no reduction reaction takes place, indicating that the products of the photoelectrochemical reaction were generated from the reduction of CO<sub>2</sub> and not from any other sources of carbon (Fig. 4). The high currents at the positive region are due to the conversion of the Ni(OH)<sub>2</sub> electrode into NiOOH, as seen in the positive electrode in NiMH batteries as specified in Eq. 3:

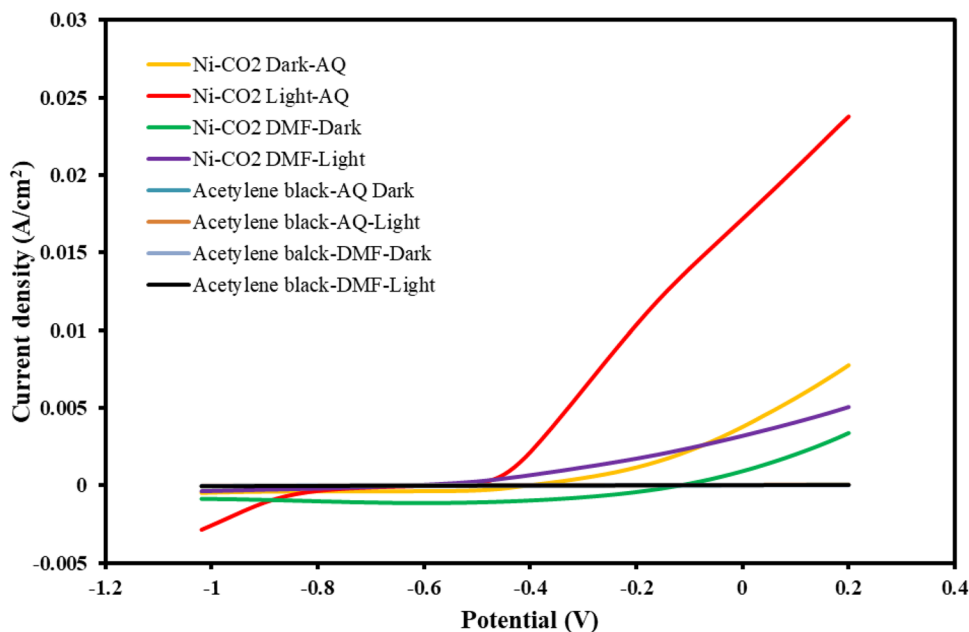


Nevertheless, the release of electrons by the Ni(OH)<sub>2</sub> electrode at a higher positive region is also due to the formation of the 'CO<sub>2</sub><sup>-</sup> radical anion in solution after accepting an electron from the conduction band upon excitation.

Based on our previous study [43], the fluctuation in the voltammetric analysis is indicative of the lower selectivity of the products. Hence, methanol, ethanol, and acetaldehyde were detected in this study during chronoamperometry (Fig. 5) in an aqueous solution (Fig. S6, ESI). Meanwhile, the steady photocurrent in DMF (Fig. 6) is indicative of the high selectivity of reduction products, which is mainly formic acid (Fig. S7, ESI). The summary of the results is tabulated in Table 1.

The amount of dissolved CO<sub>2</sub> in aqueous and DMF is determined before and after the experiment by using the titration method as mentioned in the experimental section. Before the photoelectrochemical reduction of dissolved CO<sub>2</sub>, the concentration of CO<sub>2</sub> in aqueous and DMF is 1076 and 1454 ppm, respectively. The concentration of CO<sub>2</sub> after

**Fig. 4** LSV of Ni(OH)<sub>2</sub> in aqueous (AQ) and DMF solution of 0.2 M LiClO<sub>4</sub> in dark (D) and light (L)



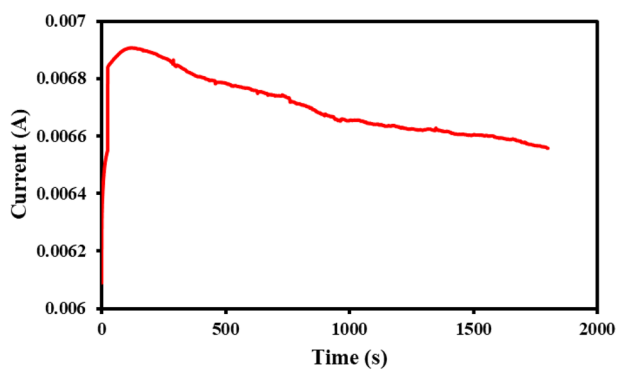


**Fig. 5** Chronoamperometry of Ni(OH)<sub>2</sub> in an aqueous solution of 0.2 M LiClO<sub>4</sub> after 6 h in light

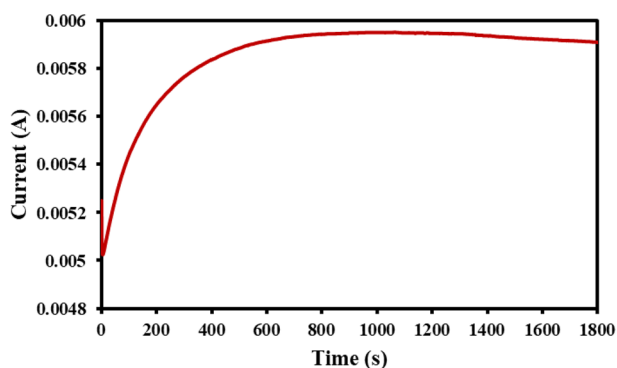


**Fig. 6** Chronoamperometry of Ni(OH)<sub>2</sub> in DMF solution of 0.2 M LiClO<sub>4</sub> + 3% H<sub>2</sub>O after 6 h in light

6 h of photoelectrochemical reduction (at  $-0.5$  V vs Ag/AgCl) in aqueous and non-aqueous medium decreased to 464 and 600 ppm, respectively. This suggests that 612 ppm and 854 ppm of products are formed during the photoelectrochemical reduction of CO<sub>2</sub> in aqueous and non-aqueous medium, respectively, after 6 h. It must be mentioned that the pH of the electrolyte also changed after the experiment in both reaction media. After 1 h of bubbling the solution with CO<sub>2</sub>, the pH in aqueous and DMF is 3.82 and 8.83, respectively. However, after 6 h of photoelectrochemical reduction, the pH of the solution changed to 7.47 and 5.83, in aqueous and DMF solution, respectively. This indicates that the increment in pH reading is due to the conversion of

formic acid into alcohols such as methanol and acetaldehyde in aqueous solution (Fig. S6, ESI), while the major product formed during the photoelectrochemical reduction of CO<sub>2</sub> in DMF medium is formic acid, detected by GCMS (Fig. S7, ESI).

After 6 h of photoelectrochemical reduction of CO<sub>2</sub>, the major reduction product in aqueous solution is acetaldehyde with a Faradaic efficiency of 24% (471 ppm) at retention time,  $R_t$  of 1.5 and 1.7 min. However, the formation of formic acid at  $R_t$  of 1.3 was also detected. The transformation of formic acid into methanol as the minor product was suggested as the main reason for the slight increment of pH value after the reaction. The Faradaic efficiency (F.E) was calculated from Eq. 4 [44]:

$$F \cdot E = \left[ (n \times z \times F) / (J_{\text{photo}} \times A \times t) \right] \times 100\% \quad (4)$$

where  $n$  is the number of moles of product generated;  $F$  is the Faraday constant with a value of  $96\,485$  C mol<sup>-1</sup>;  $z$  is the number of electrons involved;  $J_{\text{photo}}$  is the photocurrent density (A cm<sup>-2</sup>) generated during the measurement time ( $t$ ) (seconds); and  $A$  is the illumination area of the photoelectrode (cm<sup>2</sup>).

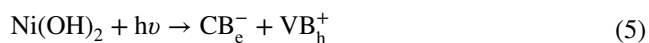
Meanwhile, formic acid appears at  $R_t$  of 1.487 min during the photoelectrochemical reduction of CO<sub>2</sub> in DMF (Fig. S7, ESI) with the Faradaic efficiency of 33%. The formation of methanol in DMF is almost not detected even after 6 h reaction due to the low amount of water (3%) content in the reaction medium, in addition to the competition with the hydrogen evolution reaction (HER) from water oxidation and the re-oxidation of product into CO<sub>2</sub>. Therefore, formic acid is regarded as the major product from the photoelectrochemical reduction of CO<sub>2</sub> in DMF.

The photochemical reduction mechanism of CO<sub>2</sub> to produce formic acid and methanol is still unclear. Two mechanisms describe the reduction of CO<sub>2</sub>, namely the formaldehyde pathway [45] and the carbene pathway [46]. Ji et al. [45] proposed that formic acid and formaldehyde could be formed according to the formaldehyde pathway which is thermodynamically feasible [47] and these products could be desorbed from the surface of the catalyst into the solution upon the reduction reaction [26, 48]. Upon light illumination, photogenerated charge carriers will be produced

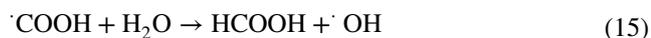
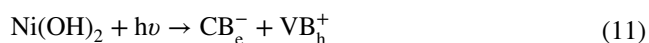
**Table 1** Chronoamperometry results of 6 h of photoelectrochemical reduction at Ni(OH)<sub>2</sub> the electrode at  $-0.5$  V (vs. Ag/AgCl) of dissolved CO<sub>2</sub> in aqueous and DMF solution

Conditions	Aqueous 0.2 M LiClO <sub>4</sub> solution	0.2 M LiClO <sub>4</sub> in DMF + 3% H <sub>2</sub> O solution
Concentration of CO <sub>2</sub> after 1 h bubbling	1076 ppm	1454 ppm
Concentration of CO <sub>2</sub> after 6 h reduction	464 ppm	600 ppm
Major product concentration	612 ppm	854 ppm
Major product	Acetaldehyde	Formic acid
Minor product	Formic acid Methanol	Methanol

where the electrons with higher energy than the bandgap of Ni(OH)<sub>2</sub> will be promoted to the conduction band leaving the photogenerated holes in the valence band. In most cases, the initial step of activation of dissolved CO<sub>2</sub> in the solution is the establishment of  $\cdot\text{CO}_2^-$  radical anion after accepting an electron from the conduction band [49]. The adsorption of  $\cdot\text{CO}_2^-$  through monodentate binding is through one of the oxygen atom or carbon atom which favors the production of the carboxylate radical ( $\cdot\text{COOH}$ ) [50]. The hydrogen radical ( $\cdot\text{H}$ ) initiated from the reduction of the proton will further react with  $\cdot\text{COOH}$  to yield HCOOH [51, 52]. The proposed reaction mechanism for formic acid production is via the formation of  $\cdot\text{CO}^-$  and  $\cdot\text{COOH}$  as the intermediate species. This is a favorable reaction pathway as reported by Habisreutinger et al. [26], since the CO<sub>2</sub> reduction in this study proceeds in a high dielectric medium such as an aqueous solution. The proposed reaction mechanism for the establishment of HCOOH is shown in [26].

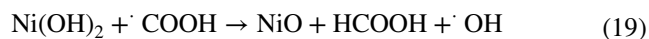
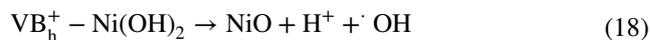


We proposed also an alternate pathway which involves the  $\cdot\text{OH}$  intermediate:

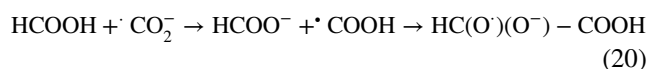


On the other hand, from the XRD results (Fig. 1) after 6 h of the photoelectrochemical reduction reaction, some

Ni(OH)<sub>2</sub> was transformed into NiO (JCPDS #47-1049) with a distinct peak at 44° in Fig. 1. The water content in Ni(OH)<sub>2</sub> is an important source for the CO<sub>2</sub> reduction to release formic acid (Eqs. 10 and 16). Hence, Ni(OH)<sub>2</sub> in the present study can be suggested as a suitable candidate for CO<sub>2</sub> reduction reaction into valuable organic oxygenates. Furthermore, we also proposed the formation of NiO from Ni(OH)<sub>2</sub> through Eqs. 18 and 19 driven by the reaction from Eqs. 14 and 16 as supported by the XRD analysis in Fig. 1.



The production of acetaldehyde is unclear, but the combination of formic acid and  $\cdot\text{CO}_2^-$  radical anion could be the major step in the formation of acetaldehyde. Furthermore, the production of acetaldehyde is proposed due to the reduction of acetic acid according to Eq. 20, although undetected by GCMS. The presence of reductants such as the conduction band electrons (CB<sub>e</sub><sup>-</sup>), H<sup>+</sup>, water, and Ni(OH)<sub>2</sub> could play a major role in the further reduction to eliminate the oxygen atoms to produce acetaldehyde in an aqueous solution.



## Conclusions

In summary, the photoelectrochemical reduction of CO<sub>2</sub> in the visible region has been studied in the aqueous and non-aqueous medium by using Ni(OH)<sub>2</sub> photocathode which has been fabricated by using the hydrothermal method. The optimum ratio for the fabrication of the photoelectrode of Ni(OH)<sub>2</sub> is 8:1:1 ratio of Ni(OH)<sub>2</sub>/PVDF/acetylene black. The prepared Ni(OH)<sub>2</sub> photocathode showed excellent photocatalytic properties over CO<sub>2</sub> reduction with a high photocurrent density of 24 mA cm<sup>-2</sup> was obtained in the aqueous solution of 0.2 M LiClO<sub>4</sub> as compared to 5 mA cm<sup>-2</sup> in DMF solution. The Faradaic efficiencies were 24 and 33% in the aqueous and DMF, respectively. Better absorption of visible light irradiation of the prepared Ni(OH)<sub>2</sub> photocathode might be due to low bandgap energy of 1.8 eV which led to better photocatalytic properties toward CO<sub>2</sub> reduction into organic oxygenates. Apart from the formation of  $\cdot\text{CO}_2^-$  radical anion as the intermediate species for the dissolved CO reduction in both aqueous and non-aqueous medium, the presence of OH-group from the transformation of Ni(OH)<sub>2</sub> was paramount important for the production of organic oxygenates such as methanol, formic acid, and acetaldehyde. Therefore, this study revealed that Ni(OH)<sub>2</sub>

could be a suitable candidate for green energy generation especially for the photoelectrochemical reduction of CO<sub>2</sub> into organic chemicals.

**Acknowledgments** The authors would like to thank University of Malaya and the Ministry of Higher Education Malaysia for funding this research through Grants RP020D-16SUS and FP039-2016.

### Compliance with ethical standards

**Conflict of interest** All authors declare that there is no conflicting interest and look forward to your positive response.

### References

- Z. He, J. Tang, J. Shen, J. Chen, S. Song, Enhancement of photocatalytic reduction of CO<sub>2</sub> to CH<sub>4</sub> over TiO<sub>2</sub> nanosheets by modifying with sulfuric acid. *Appl. Surf. Sci.* **364**, 416–427 (2016)
- Q. Zhang, J. Du, A. He, Z. Liu, C. Tao, Low overpotential electrochemical CO<sub>2</sub> reduction to formate on Co<sub>3</sub>O<sub>4</sub>-CeO<sub>2</sub>/low graphitic carbon catalyst with oxygen vacancies. *J. Solid State Chem.* **279**, 120946–120954 (2019)
- E. Szaniawska, K. Bienkowski, I.A. Rutkowska, P.J. Kulesza, R. Solarska, Enhanced photoelectrochemical CO<sub>2</sub>-reduction system based on mixed Cu<sub>2</sub>O–nonstoichiometric TiO<sub>2</sub> photocathode. *Catal. Today* **300**, 145–151 (2018)
- N.T.T. Truc, L.G. Bach, N.T. Hanh, T.-D. Pham, N.T.P. Le Chi, D.T. Tran, M.V. Nguyen, V.N. Nguyen, The superior photocatalytic activity of Nb doped TiO<sub>2</sub>/g-C<sub>3</sub>N<sub>4</sub> direct Z-scheme system for efficient conversion of CO<sub>2</sub> into valuable fuels. *J. Colloid Interface Sci.* **540**, 1–8 (2019)
- L. Yu, X. Ba, M. Qiu, Y. Li, L. Shuai, W. Zhang, Z. Ren, Y. Yu, Visible-light driven CO<sub>2</sub> reduction coupled with water oxidation on Cl-doped Cu<sub>2</sub>O nanorods. *Nano Energy* **60**, 576–582 (2019)
- D.H. Apaydin, E. Tordin, E. Portenkirchner, G. Aufischer, S. Schlager, M. Weichselbaumer, K. Oppelt, N.S. Sariciftci, Photoelectrochemical Reduction of CO<sub>2</sub> Using Third-Generation Conjugated Polymers. *ChemistrySelect* **1**, 1156–1162 (2016)
- S. Kaneco, H. Katsumata, T. Suzuki, K. Ohta, Electrochemical reduction of CO<sub>2</sub> to methane at the Cu electrode in methanol with sodium supporting salts and its comparison with other alkaline salts. *Energy Fuels* **20**, 409–414 (2006)
- J. Qu, X. Zhang, Y. Wang, C. Xie, Electrochemical reduction of CO<sub>2</sub> on RuO<sub>2</sub>/TiO<sub>2</sub> nanotubes composite modified Pt electrode. *Electrochim. Acta* **50**, 3576–3580 (2005)
- N. Furuya, S. Koide, Electroreduction of carbon dioxide by metal phthalocyanines. *Electrochim. Acta* **36**, 1309–1313 (1991)
- A.A. Peterson, J.K. Nørskov, Activity descriptors for CO<sub>2</sub> electroreduction to methane on transition-metal catalysts. *J. Phys. Chem. Lett.* **3**, 251–258 (2012)
- T. Yamamoto, D.A. Tryk, A. Fujishima, H. Ohata, Production of syngas plus oxygen from CO<sub>2</sub> in a gas-diffusion electrode-based electrolytic cell. *Electrochim. Acta* **47**, 3327–3334 (2002)
- Y. Zhang, L. Sun, K. Lv, Y. Zhang, One-pot synthesis of Ni(OH)<sub>2</sub> flakes embedded in highly-conductive carbon nanotube/graphene hybrid framework as high performance electrodes for supercapacitors. *Mater. Lett.* **213**, 131–134 (2018)
- H. Wu, Y. Li, J. Ren, D. Rao, Q. Zheng, L. Zhou, D. Lin, CNT-assembled dodecahedra core@ nickel hydroxide nanosheet shell enabled sulfur cathode for high-performance lithium-sulfur batteries. *Nano Energy* **55**, 82–92 (2019)
- V. Ganesh, S. Farzana, S. Berchmans, Nickel hydroxide deposited indium tin oxide electrodes as electrocatalysts for direct oxidation of carbohydrates in alkaline medium. *J. Power Sources* **196**, 9890–9899 (2011)
- S. Ramesh, K. Karuppasamy, H.M. Yadav, J.-J. Lee, H.-S. Kim, H.-S. Kim, J.-H. Kim, Ni(OH)<sub>2</sub>-decorated nitrogen doped MWCNT nanosheets as an efficient electrode for high performance supercapacitors. *Sci. Rep.* **9**, 1–10 (2019)
- X. Zhou, Z. Xia, Z. Zhang, Y. Ma, Y. Qu, One-step synthesis of multi-walled carbon nanotubes/ultra-thin Ni(OH)<sub>2</sub> nanoplate composite as efficient catalysts for water oxidation. *J. Mater. Chem. A* **2**, 11799–11806 (2014)
- H. Zhou, J. Peng, X. Qiu, Y. Gao, L. Lu, W. Wang, β-Ni(OH)<sub>2</sub> nanosheets: an effective sensing platform for constructing nucleic acid-based optical sensors. *J. Mater. Chem. B* **5**, 7426–7432 (2017)
- Q. Xu, H. Jiang, H. Zhang, Y. Hu, C. Li, Heterogeneous interface engineered atomic configuration on ultrathin Ni(OH)<sub>2</sub>/Ni<sub>3</sub>S<sub>2</sub> nanoforests for efficient water splitting. *Appl. Catal. B* **242**, 60–66 (2019)
- I. Vamvasakis, I.T. Papadas, T. Tzanoudakis, C. Drivas, S.A. Choulis, S. Kennou, G.S. Armatas, Visible-light photocatalytic H<sub>2</sub> production activity of β-Ni(OH)<sub>2</sub>-modified CdS mesoporous nanoheterojunction networks. *ACS Catal.* **8**, 8726–8738 (2018)
- N.I.M. Abdallah, Y. Li, X.-T. Wang, X. Li, C.-W. Wang, Design and fabrication of Ni(OH)<sub>2</sub>/BiVO<sub>4</sub> heterostructured nano-photocatalyst for high-efficient removal of organic dyes. *J. Alloys Compd.*, (2020) 154828–154836
- M. Barakat, M. Anjum, R. Kumar, Z. Alafif, M. Oves, M.O. Ansari, Design of ternary Ni(OH)<sub>2</sub>/graphene oxide/TiO<sub>2</sub> nanocomposite for enhanced photocatalytic degradation of organic, microbial contaminants, and aerobic digestion of dairy wastewater. *J. Clean. Prod.* **258**, 120588–120597 (2020)
- A. Meng, S. Wu, B. Cheng, J. Yu, J. Xu, Hierarchical TiO<sub>2</sub>/Ni(OH)<sub>2</sub> composite fibers with enhanced photocatalytic CO<sub>2</sub> reduction performance. *J. Mater. Chem. A* **6**, 4729–4736 (2018)
- S. Palanisamy, S. Srinivasan, Electrochemical reduction of CO<sub>2</sub> on Ni(OH)<sub>2</sub> doped water dispersible graphene under different electrolyte conditions. *SN Appl. Sci.* **1**, 837–843 (2019)
- L. Dai, Q. Qin, P. Wang, X. Zhao, C. Hu, P. Liu, R. Qin, M. Chen, D. Ou, C. Xu, Ultrastable atomic copper nanosheets for selective electrochemical reduction of carbon dioxide. *Sci. Adv.* **3**, e1701069–e1701078 (2017)
- M.S. Akple, T. Ishigaki, P. Madhusudan, Bio-inspired honeycomb-like graphitic carbon nitride for enhanced visible light photocatalytic CO<sub>2</sub> reduction activity. *Environ. Sci. Pollut. Res.*, (2020) 1–15
- S.N. Habisreutinger, L. Schmidt-Mende, J.K. Stolarczyk, Photocatalytic reduction of CO<sub>2</sub> on TiO<sub>2</sub> and other semiconductors. *Angew. Chem. Int. Ed.* **52**, 7372–7408 (2013)
- L. Kong, Z. Jiang, H.H. Lai, R.J. Nicholls, T. Xiao, M.O. Jones, P.P. Edwards, Unusual reactivity of visible-light-responsive AgBr–BiOBr heterojunction photocatalysts. *J. Catal.* **293**, 116–125 (2012)
- X.-J. Wen, C.-G. Niu, M. Ruan, L. Zhang, G.-M. Zeng, AgI nanoparticles-decorated CeO<sub>2</sub> microspheres photocatalyst for the degradation of organic dye and tetracycline under visible-light irradiation. *J. Colloid Interface Sci.* **497**, 368–377 (2017)
- Y. Qi, H. Qi, C. Lu, Y. Yang, Y. Zhao, Photoluminescence and magnetic properties of β-Ni(OH)<sub>2</sub> nanoplates and NiO nanostructures. *J. Mater. Sci.: Mater. Electron.* **20** (2009) 479–483
- G. Lakshminarayana, S. Buddhudu, Spectral analysis of Mn<sup>2+</sup>, Co<sup>2+</sup> and Ni<sup>2+</sup>: B<sub>2</sub>O<sub>3</sub>-ZnO-PbO glasses. *Spectrochim. Acta Part A* **63**, 295–304 (2006)
- A. De Moura, R. Lima, E. Paris, M. Li, J.A. Varela, E. Longo, Formation of β-nickel hydroxide plate-like structures under mild

- conditions and their optical properties. *J. Solid State Chem.* **184**, 2818–2823 (2011)
32. Z. Liu, R. Ma, M. Osada, K. Takada, T. Sasaki, Selective and controlled synthesis of  $\alpha$ - and  $\beta$ -cobalt hydroxides in highly developed hexagonal platelets. *J. Am. Chem. Soc.* **127**, 13869–13874 (2005)
  33. D. Dubal, V. Fulari, C. Lokhande, Effect of morphology on supercapacitive properties of chemically grown  $\beta$ -Ni(OH)<sub>2</sub> thin films. *Microporous Mesoporous Mater.* **151**, 511–516 (2012)
  34. M. Chatterjee, D. Enkhtuvshin, B. Siladitya, D. Ganguli, Hollow alumina microspheres from boehmite sols. *J. Mater. Sci.* **33**, 4937–4942 (1998)
  35. S. Tamura, A. Mori, N. Imanaka, Li<sup>+</sup> ion conduction in (Gd, La)<sub>2</sub>O<sub>3</sub>–LiNO<sub>3</sub> system. *Solid State Ion.* **175**, 467–470 (2004)
  36. M. Sulaiman, A. Rahman, N. Mohamed, Effect of water-based sol gel method on structural, thermal and conductivity properties of LiNO<sub>3</sub>–Al<sub>2</sub>O<sub>3</sub> composite solid electrolytes. *Arab. J. Chem.* **10**, 1147–1152 (2017)
  37. T. Ramesh, P.V. Kamath, Synthesis of nickel hydroxide: effect of precipitation conditions on phase selectivity and structural disorder. *J. Power Sources* **156**, 655–661 (2006)
  38. P. Jeevanandam, Y. Koltypin, A. Gedanken, Synthesis of nano-sized  $\alpha$ -nickel hydroxide by a sonochemical method. *Nano Lett.* **1**, 263–266 (2001)
  39. D. Yang, R. Wang, M. He, J. Zhang, Z. Liu, Ribbon- and board-like nanostructures of nickel hydroxide: synthesis, characterization, and electrochemical properties. *J. Phys. Chem. B* **109**, 7654–7658 (2005)
  40. E. Shangguan, H. Tang, Z. Chang, X.-Z. Yuan, H. Wang, Effects of different Ni(OH)<sub>2</sub> precursors on the structure and electrochemical properties of NiOOH. *Int. J. Hydrog. Energy* **36**, 10057–10064 (2011)
  41. M.K. Motlagh, A. Youzbashi, F. Hashemzadeh, L. Sabaghzadeh, Structural properties of nickel hydroxide/oxyhydroxide and oxide nanoparticles obtained by microwave-assisted oxidation technique. *Powder Technol.* **237**, 562–568 (2013)
  42. M. Zhou, Z. Wei, H. Qiao, L. Zhu, H. Yang, T. Xia, Particle size and pore structure characterization of silver nanoparticles prepared by confined arc plasma. *J. Nanomater.* **2009**, 3 (2009)
  43. M.R. Hasan, S.B.A. Hamid, W.J. Basirun, S.H.M. Suhaimy, A.N.C. Mat, A sol–gel derived, copper-doped, titanium dioxide-reduced graphene oxide nanocomposite electrode for the photoelectrocatalytic reduction of CO<sub>2</sub> to methanol and formic acid. *RSC Adv.* **5**, 77803–77813 (2015)
  44. C. Jiang, J. Wu, S.J. Moniz, D. Guo, M. Tang, Q. Jiang, S. Chen, H. Liu, A. Wang, T. Zhang, Stabilization of GaAs photoanodes by in situ deposition of nickel-borate surface catalysts as hole trapping sites. *Sustain. Energy Fuels* **3**, 814–822 (2019)
  45. Y. Ji, Y. Luo, Theoretical Study on the Mechanism of Photoreduction of CO<sub>2</sub> to CH<sub>4</sub> on the Anatase TiO<sub>2</sub> (101) Surface. *ACS Catal.* **6**, 2018–2025 (2016)
  46. S.t. Neațu, J.A. Maciá-Agulló, P. Concepción, H. Garcia, Gold–copper nanoalloys supported on TiO<sub>2</sub> as photocatalysts for CO<sub>2</sub> reduction by water. *J. Am. Chem. Soc.*, 136 (2014) 15969–15976
  47. J. Mao, K. Li, T. Peng, Recent advances in the photocatalytic CO<sub>2</sub> reduction over semiconductors. *Catal. Sci. Technol.* **3**, 2481–2498 (2013)
  48. N. Zhang, R. Long, C. Gao, Y. Xiong, Recent progress on advanced design for photoelectrochemical reduction of CO<sub>2</sub> to fuels. *Sci. China Mater.* **61**, 771–805 (2018)
  49. J.L. White, M.F. Baruch, J.E. Pander III, Y. Hu, I.C. Fortmeyer, J.E. Park, T. Zhang, K. Liao, J. Gu, Y. Yan, Light-driven heterogeneous reduction of carbon dioxide: photocatalysts and photoelectrodes. *Chem. Rev.* **115**, 12888–12935 (2015)
  50. M. Gattrell, N. Gupta, A. Co, A review of the aqueous electrochemical reduction of CO<sub>2</sub> to hydrocarbons at copper. *J. Electroanal. Chem.* **594**, 1–19 (2006)
  51. M. Subrahmanyam, S. Kaneco, N. Alonso-Vante, A screening for the photo reduction of carbon dioxide supported on metal oxide catalysts for C<sub>1</sub>–C<sub>3</sub> selectivity. *Appl. Catal. B* **23**, 169–174 (1999)
  52. N. Sasirekha, S.J.S. Basha, K. Shanthi, Photocatalytic performance of Ru doped anatase mounted on silica for reduction of carbon dioxide. *Appl. Catal. B* **62**, 169–180 (2006)